



# Determining inter-system bias of GNSS signals with narrowly spaced frequencies for GNSS positioning

Yumiao Tian<sup>1,2,3</sup> · Zhizhao Liu<sup>2</sup> · Maorong Ge<sup>4</sup> · Frank Neitzel<sup>3</sup>

Received: 7 June 2017 / Accepted: 4 December 2017 / Published online: 14 December 2017  
© Springer-Verlag GmbH Germany, part of Springer Nature 2017

## Abstract

Relative positioning using multi-GNSS (global navigation satellite systems) can improve accuracy, reliability, and availability compared to the use of a single constellation system. Intra-system double-difference (DD) ambiguities (ISDDAs) refer to the DD ambiguities between satellites of a single constellation system and can be fixed to an integer to derive the precise fixed solution. Inter-system ambiguities, which denote the DD ambiguities between different constellation systems, can also be fixed to integers on overlapping frequencies, once the inter-system bias (ISB) is removed. Compared with fixing ISDDAs, fixing both integer intra- and inter-system DD ambiguities (IIDDAs) means an increase of positioning precision through an integration of multiple GNSS constellations. Previously, researchers have studied IIDDAs with systems of the same frequencies, but not with systems of different frequencies. Integer IIDDAs can be determined from single-difference (SD) ambiguities, even if the frequencies of multi-GNSS signals used in the positioning are different. In this study, we investigated IIDDAs for multi-GNSS signals of narrowly spaced frequencies. First, the inter-system DD models of multi-GNSS signals of different frequencies are introduced, and the strategy for compensating for ISB is presented. The ISB is decomposed into three parts: 1) a float approximate ISB number that can be considered equal to the ISB of code pseudorange observations and thus can be estimated through single point positioning (SPP); 2) a number that is a multiple of the GNSS signal wavelength; and 3) a fractional ISB part, with a magnitude smaller than a single wavelength. Then, the relationship between intra- and inter-system DD ambiguity RATIO values and ISB was investigated by integrating GPS L1 and GLONASS L1 signals. In our numerical analyses with short baselines, the ISB parameter and IIDDAs were successfully fixed, even if the number of observed satellites in each system was small.

**Keywords** Multi-GNSS integration · Narrowly spaced frequencies · Inter-system bias · Inter-system DD ambiguity fixing · Intra-system DD ambiguity fixing

## 1 Introduction

Global navigation satellite system (GNSS) is a powerful tool for precise positioning and navigation. In addition to

the fully operational Global Positioning System (GPS) and GLObal NAVigation Satellite System (GLONASS), new systems, such as the European Galileo, Chinese BeiDou Navigation Satellite System (BDS), Japanese Quasi-Zenith Satellite System (QZSS), and the Indian NAVigation with Indian Constellation (NAVIC) systems, have been developed (Montenbruck et al. 2014; Nadarajah et al. 2015). In total, these systems incorporate more than 100 satellites and nearly 20 carrier frequencies (Table 1). Integration of these multi-GNSS signals can improve positioning accuracy, reliability, and availability (Li et al. 2015; Wang et al. 2001; Force and Miller 2013). In relative positioning mode, a double-difference (DD) observation model between receivers and satellites is used to reduce or eliminate the observation errors in un-difference observations. In this paper, “intra-system” refers to DD model/observations between satellites of the

✉ Zhizhao Liu  
lszzliu@polyu.edu.hk

<sup>1</sup> Faculty of Geosciences and Environmental Engineering, Southwest Jiaotong University, Chengdu, Sichuan 610031, China

<sup>2</sup> Department of Land Surveying and Geo-Informatics, Hong Kong Polytechnic University, Hong Kong, China

<sup>3</sup> Institute of Geodesy and Geoinformation Science, Technische Universität Berlin, 10623 Berlin, Germany

<sup>4</sup> German Research Centre for Geosciences, 14473 Potsdam, Germany

**Table 1** Frequencies used by GNSS

	a	b	c	d	e	f	g	h	i	J	k	l	m	n	o	p	q	r	s
L1(GLO-RF) a	■	✘	✘	✘															
L1(GPS) b	✘	■	■	■	○														
L1(QZSS) c	✘	■	■	■	○														
E1 d	✘	■	■	■	○														
B1 e		○	○	○	■														
E6 f						■	■	○											
LEX g						■	■	○											
B3 h						○	○	■											
L2(GLO-RF) i									■	✘	✘								
L2(GPS) j									✘	■	■								
L2(QZSS) k									✘	■	■								
E5B l												■	■	○	✘				
B2 m												■	■	○	✘				
L3(GLO-RC) n												○	○	■	△				
E5 o												✘	✘	△	■	✘	✘	✘	✘
L5(GPS) p															✘	■	■	■	■
L5(QZSS) q															✘	■	■	■	■
E5a r															✘	■	■	■	■
SPS-L5 s															✘	■	■	■	■

GLO-RF refers to a GLONASS FDMA frequency band; RC refers to a CDMA GLONASS frequency band; red squares indicate DDs of identical GNSS signals; green squares indicate DDs of GNSS signals of the same frequencies from different GNSS systems; yellow squares indicate DDs of GNSS signals of different frequencies with wavelength differences smaller than 4 mm, where  $1\text{ mm} < \circ < 2\text{ mm} < \Delta < 3\text{ mm} < \text{✘} < 4\text{ mm}$

same system. Intra-system DD fixing has been extensively studied, especially for the GPS intra-system signals. “Inter-system” denotes DD model/observations between different satellite systems. Inter-system DD models enable observations from different systems to be processed together in a single mathematical model. This results in improved integer ambiguity resolution, and consequently more reliable positioning results (Julien et al. 2003; Odijk and Teunissen 2013a). However, fixing DD ambiguities to integer values in inter-system DD models requires that the inter-system bias (ISB) be known or estimated. The ISB is mainly composed of hardware delays, resulting from different signal paths in the GNSS devices (Odijk and Teunissen 2013b; Paziewski and Wielgosz 2015; Wang et al. 2001).

In the construction of inter-system DD models, observations of the same frequencies, such as GPS and Galileo L1-E1 and L5-E5a, are preferred (Odijk and Teunissen 2013a; Odijk et al. 2014; Odolinski et al. 2014; Julien et al. 2003). In this case, single-difference (SD) ambiguities from different systems can be directly combined to produce integer DD ambiguities. These integer inter-system DD ambiguities can be resolved once the ISB is known. The ISB can be regarded as a combination of an integer part and a fractional part. The

integer part is a multiple of the wavelength of the GNSS signal and can be combined with integer DD ambiguities without affecting the performance of final positioning performance. The fractional part (F-ISB) is a fraction of the wavelength and needs to be accurately estimated. However, when the F-ISB is estimated as an unknown parameter in the DD model, the normal equation (NEQ) in the data processing is rank deficient because the number of SD ambiguities is one more than the number of DD equations. Methods have been proposed to eliminate this rank deficiency problem. For instance, Odijk and Teunissen (2013b) estimated the F-ISB by selecting a reference satellite for each system and fixing only integer intra-system DD ambiguities (ISD-DAs). Paziewski and Wielgosz (2015) added a constraint to the equation by assigning the F-ISB parameter an a priori value. Tian et al. (2016) proposed a particle filter approach, which fixed both integer intra- and inter-system DD ambiguities (IIDDAs) in F-ISB estimation via pregenerated F-ISB samples.

However, in multi-GNSS applications, a large proportion of GNSS signals have different frequencies. Many of these frequencies are narrowly spaced, as shown in Table 1. For instance, BeiDou B1 and GPS L1 have a wavelength differ-

ence of 1.7 mm, BeiDou B3 and Galileo E6 have a difference of 1.9 mm, and Galileo E5b and GLONASS L3 have a difference of 1.1 mm. When GNSS signals of different frequencies are used together in relative positioning, SD ambiguities cannot be directly combined to form integer DD ambiguities. This is similar to the case of processing data from a frequency-division multiple access (FDMA) GLONASS system (Leick 1998; Wang et al. 2001). Ambiguity resolution in GLONASS data processing has been investigated previously. However, an inter-system model with narrowly spaced frequencies has not yet been reported. Therefore, we investigated such a model and developed a strategy similar to that of processing FDMA-based GLONASS data with corrected ISB to fix IIDDAs. The developed strategy is generic and can be applied to multi-GNSS integration with both FDMA and CDMA (code-division multiple access) techniques.

We first analyzed the relationship between RATIO and ISB variables to develop a strategy to determine ISB parameters in an inter-system model. RATIO was defined as the ratio of the secondary candidate of minimum  $q(b)$  to the primary candidate of minimum  $q(b)$  (Euler and Schaffrin 1991).  $q(b) = (\hat{b} - b)^T Q_{\hat{b}\hat{b}}^{-1} (\hat{b} - b)$ , where  $\hat{b}$  and  $Q_{\hat{b}\hat{b}}$  are the float DD ambiguity vector and the corresponding variance–covariance (VC) matrix, respectively, and  $b$  is integer-ambiguity-vector candidate. RATIO values reflect the closeness of the float ambiguity solution to its nearest integer vector (Verhagen and Teunissen 2013). Hence, they can be used to analyze ambiguity resolution performance.

In the developed strategy, the ISB  $\mu$  in the inter-system model is separated into three parts, the approximate ISB part  $d$ , the integer part  $\lambda N$  with  $\lambda$  being the carrier phase wavelength, and the remaining F-ISB  $\delta\mu$ . Therefore, we have  $\mu = d + \lambda N + \delta\mu$ . Once the approximate ISB part is obtained, it is used to remove the major effect of the ISB on the carrier phase of the inter-system model. The integer part represents the part whose value is an integer number of wavelengths and can therefore be neglected since it becomes a part of integer ambiguity. The remaining F-ISB value is estimated by locally maximizing the RATIO value in integer DD ambiguity resolution. To obtain an accurate F-ISB value, the particle filter approach (Doucet et al. 2001; Gordon et al. 1993; Tian et al. 2015) is used in this study. After the approximate ISB and accurate F-ISB values are obtained, they are added together to obtain a final ISB value, which enables the resolution of integer IIDDAs.

In the experiments, we chose to use the GPS L1 (1575.42 MHz) and GLONASS L1 (1598.0625–1605.375 MHz) signals to build the inter-system DD model. These frequency bands were selected because the largest wavelength difference between them is 3.55 mm, which is large enough to study integer DD ambiguity resolution and F-ISB estimation through the analysis of RATIO value characteris-

tics. In addition, larger wavelength differences require more accurate initial SD phase ambiguities. If the wavelength difference is too large, the initial SD phase ambiguities calculated from low-accuracy pseudorange observations may not be sufficiently accurate. This wavelength difference allows observing solution improvements for short baselines such as 10–15 km. Moreover, both GPS and GLONASS constellations are fully operational. Therefore, a large number of GPS and GLONASS satellites can be used to study integer DD ambiguity resolution, F-ISB estimation, and RATIO value distribution characteristics. Furthermore, the strategy developed for FDMA signals can also be applied to CDMA signals, because CDMA signals can be regarded as a special case of FDMA signals in terms of their hardware delays.

This paper is organized as follows. Section 2 presents the mathematic models for multi-GNSS integration. Section 3 details the relationship between RATIO and F-ISB values. Section 4 describes the experimental and analytical results. Our conclusions are given in Sect. 5.

## 2 Intra- and inter-system double-difference models and estimation of F-ISB

Because of passing through different hardware channels or being processed differently by the firmware of receivers, GNSS signals from different constellations and different GLONASS FDMA frequencies are affected by multi-GNSS ISB and GLONASS inter-frequency bias (IFB), respectively (Melgard et al. 2013). In DD observation models, the between-receiver hardware delays do not cancel out and they need to be estimated (Al-Shaery et al. 2012; Wanninger 2012; Cai and Gao 2013; Odijk et al. 2014).

For GLONASS FDMA signals, the GLONASS IFB present in the code pseudorange and carrier phase observations may be nonzero in the DD model. This effect has been demonstrated using two receivers from different manufacturers (Wanninger 2012; Paziewski and Wielgosz 2015). The effects of the remaining hardware delays on pseudorange observations are difficult to model. However, the effects on carrier phase observations have been found to be linear with respect to the channel number and can be precisely expressed by a constant value plus its rate term (Wanninger 2012; Tian et al. 2015). For instance, the carrier phase IFB  $\mu_a^i$  for a station  $a$  and satellite  $i$  can be described as  $\mu_a^i = \bar{\mu}_a + k^i \Delta\gamma_{a,\text{FDMA}}$ , where  $\bar{\mu}_a$  is the constant and  $\Delta\gamma_{a,\text{FDMA}}$  is the rate of change with channel number  $k^i$ .

Considering the GLONASS IFB, the generic un-difference GNSS observation model can be expressed as follows (Teunissen and Kleusberg 1998):

$$P_a^{s1,i} = \rho_a^{s1,i} - c(\delta t_a - \delta t^{s1,i}) + \bar{d}_a^{s1} + \Delta d_{a,FDMA}^i - d^{s1,i} + I_a^{s1,i} + T_a^{s1,i} + cal_a^{s1,i} + M_a^{s1,i} + \varepsilon_a^{s1,i} \tag{1a}$$

$$\lambda^{s1,i} \Phi_a^{s1,i} = \rho_a^{s1,i} - c(\delta t_a - \delta t^{s1,i}) + \bar{\mu}_a^{s1} + k^i \Delta \gamma_{a,FDMA} - \mu^{s1,i} - I_a^{s1,i} + T_a^{s1,i} + cal_a^{s1,i} + m_a^{s1,i} + \lambda^{s1,i} N_a^{s1,i} + \lambda^{s1,i} \psi_a^{s1,i} + \xi_a^{s1,i}, \tag{1b}$$

where  $s1$  denotes a GNSS constellation system, such as GPS, GLONASS, or Galileo.  $P_a^i$  is the pseudorange code observation (m).  $\Phi_a^i$  is the carrier phase observation (cycles). Superscript  $i$  and subscript  $a$  refer to the GNSS satellite and receiver, respectively.  $\lambda^i$  is the wavelength of the carrier phase observation (m/cycle).  $\rho_a^i$  refers to the geometric distance between the phase centers of the satellite and receiver antennas (m).  $c$  is the speed of light in a vacuum (m/s).  $\delta t_a$  and  $\delta t^i$  are the clock offsets for the receiver and satellite, respectively (s).  $\bar{d}_a$  and  $\bar{\mu}_a$  are the common parts of the receiver hardware delays for all of the satellites in a constellation system for pseudorange and phase observations, respectively (m).  $\Delta d_{a,FDMA}^i$  represents the remainder of the receiver hardware delay, on top of the  $\bar{d}_a$  in pseudorange observations (m).  $k^i$  is the slot number of the GLONASS satellite.  $\Delta \gamma_{a,FDMA}$  is the IFB rate for GLONASS phase observations (m).  $\Delta d_{a,FDMA}^i$  and  $\Delta \gamma_{a,FDMA}$  have values of zero for CDMA signals.  $d^i$  and  $\mu^i$  represent the satellite bias delays in pseudorange and carrier phase observations, respectively.  $I_a^i$  and  $T_a^i$  are the ionospheric and tropospheric delays, respectively (m).  $cal_a^i$  includes the errors such as earth tide, ocean loading, relativity effects, antenna phase center offset/variation and phase windup effects, and so on (m). Those errors can be accurately modeled in the data processing.  $M_a^i$  and  $m_a^i$  are the multipath effects in the pseudorange and carrier phase observations, respectively (m).  $N_a^i$  is the carrier phase integer ambiguity, and  $\psi_a^i$  is the initial phase (cycles).  $\varepsilon_a^i$  and  $\xi_a^i$  refer to the measurement noise for pseudorange and carrier phase observations, respectively (m).

Since the term  $cal_a^i$  can be accurately modeled, they will be neglected in the following discussion. Multipath effects are difficult to model and typically cannot be canceled by differencing. Therefore, they are treated as white noise. The satellite clock error can be canceled in the between-receiver single difference. The initial phases are correlated with hardware delays and thus are considered as a part of hardware delays and are not parameterized separately. Hence, the between-receiver SD model can be expressed as follows:

$$P_{ab}^{s1,i} = \rho_{ab}^{s1,i} - c\delta t_{ab}^{s1,i} + \bar{d}_{ab}^{s1} + \Delta d_{ab,FDMA}^i + I_{ab}^{s1,i} + T_{ab}^{s1,i} + \varepsilon_{ab}^{s1,i} \tag{2a}$$

$$\lambda^{s1,i} \Phi_{ab}^{s1,i} = \rho_{ab}^{s1,i} - c\delta t_{ab}^{s1,i} + \bar{\mu}_{ab}^{s1} + k^i \Delta \gamma_{ab,FDMA} + \lambda^{s1,i} N_{ab}^{s1,i} - I_{ab}^{s1,i} + T_{ab}^{s1,i} + \xi_{ab}^{s1,i}, \tag{2b}$$

where  $b$  represents the second receiver of a baseline. The DD model between two stations  $a$  and  $b$ , and two satellites  $i$  and  $j$ , can be given as follows:

$$P_{ab}^{s1s2,ij} = \rho_{ab}^{s1s2,ij} + \bar{d}_{ab}^{s1s2} + \Delta d_{ab,FDMA}^{ij} + I_{ab}^{s1s2,ij} + T_{ab}^{s1s2,ij} + \varepsilon_{ab}^{s1s2,ij} \tag{3a}$$

$$\lambda^{s2,j} \Phi_{ab}^{s2,j} - \lambda^{s1,i} \Phi_{ab}^{s1,i} = \rho_{ab}^{s1s2,ij} + \bar{\mu}_{ab}^{s1s2} + (k^j - k^i) \Delta \gamma_{ab,FDMA} + \lambda^{s2,j} N_{ab}^{s2,j} - \lambda^{s1,i} N_{ab}^{s1,i} - I_{ab}^{s1s2,ij} + T_{ab}^{s1s2,ij} + \xi_{ab}^{s1s2,ij} \tag{3b}$$

This is a generic DD model, where  $s1$  and  $s2$  can be either the same GNSS system or different systems, with either the same or different frequencies.

For GLONASS FDMA signals, the IFB in pseudorange observations is usually stable over time (Kozlov et al. 2000). Thus, it can be corrected using a lookup table of pseudorange SD-IFB values. To generate such a lookup table, the pseudorange IFB is first set to zero in the pseudorange DD model, and the processing residuals are obtained. These nonzero DD residuals are regarded as DD pseudorange hardware delays and modeled using SD pseudorange hardware delay parameters. The corresponding equation is rank deficient by one. Assuming that the sum of all of the SD pseudorange hardware delays equals zero, the rank deficiency problem can be resolved and the SD pseudorange hardware delays can be determined. This method of eliminating rank deficiency is the same as that utilized by Alber et al. (2000), where single-path phase delays of atmospheric water vapor were obtained from the DD values in GPS data processing. The GLONASS IFB in carrier phase observations can be estimated using the method proposed by Tian et al. (2015). After the IFB is removed in the SD or DD models, integer DD carrier phase ambiguities can be resolved.

If the GLONASS pseudorange SD-IFB and the GLONASS phase IFB have been corrected using the pseudorange IFB lookup table and the phase IFB rate, respectively, the corresponding parameters in the SD model (2) and the DD model (3) are eliminated. Therefore, these models can be rewritten as follows:

$$P_{ab}^{s1,i} = \rho_{ab}^{s1,i} - c\delta t_{ab}^{s1,i} + \bar{d}_{ab}^{s1} + I_{ab}^{s1,i} + T_{ab}^{s1,i} + \varepsilon_{ab}^{s1,i} \tag{4a}$$

$$\lambda^{s1,i} \Phi_{ab}^{s1,i} = \rho_{ab}^{s1,i} - c\delta t_{ab}^{s1,i} + \bar{\mu}_{ab}^{s1} + \lambda^{s1,i} N_{ab}^{s1,i} - I_{ab}^{s1,i} + T_{ab}^{s1,i} + \xi_{ab}^{s1,i} \tag{4b}$$

and

$$P_{ab}^{s1s2,ij} = \rho_{ab}^{s1s2,ij} + \bar{d}_{ab}^{s1s2} + I_{ab}^{s1s2,ij} + T_{ab}^{s1s2,ij} + \varepsilon_{ab}^{s1s2,ij} \tag{5a}$$

$$\lambda^{s2,j} \Phi_{ab}^{s2,j} - \lambda^{s1,i} \Phi_{ab}^{s1,i} = \rho_{ab}^{s1s2,ij} + \bar{\mu}_{ab}^{s1s2} + \lambda^{s2,j} N_{ab}^{s2,j} - \lambda^{s1,i} N_{ab}^{s1,i} - I_{ab}^{s1s2,ij} + T_{ab}^{s1s2,ij} + \xi_{ab}^{s1s2,ij}. \tag{5b}$$

### 2.1 Intra-system DD model

For intra-system DD models,  $s1$  and  $s2$  represent the same system ( $s1 = s2$ ). Thus, the common parts of the hardware delays  $\bar{d}_{ab}^{s1s2}$  and  $\bar{\mu}_{ab}^{s1s2}$  in Eq. (5) cancel each other. The remaining equations for FDMA and non-FDMA satellite systems are presented in this section.

#### 2.1.1 Intra-system DD model for non-FDMA satellite systems

For the intra-system DD model, the two satellite systems in Eq. (5) are the same ( $s1 = s2$ ). If the single GNSS satellite system is a non-FDMA system, and at the same time the GNSS signals are generated at the same frequency, the two ambiguity terms in Eq. (5b) combine to form the DD ambiguity. Thus, the intra-system model can be expressed as follows:

$$P_{ab}^{s1s1,ij} = \rho_{ab}^{s1s1,ij} + I_{ab}^{s1s1,ij} + T_{ab}^{s1s1,ij} + \varepsilon_{ab}^{s1s1,ij} \tag{6a}$$

$$\lambda \Phi_{ab}^{s1s1,ij} = \rho_{ab}^{s1s1,ij} + \lambda N_{ab}^{s1s1,ij} - I_{ab}^{s1s1,ij} + T_{ab}^{s1s1,ij} + \xi_{ab}^{s1s1,ij}. \tag{6b}$$

In this case, the DD ambiguity  $N_{ab}^{s1s1,ij}$  is an integer. If the float values of  $N_{ab}^{s1s1,ij}$  and the corresponding VC matrix are estimated, the integer DD ambiguities can be fixed using the integer least squares method.

#### 2.1.2 Intra-system DD model for FDMA satellite systems

When two FDMA signals are used to form DD, the difference between their wavelengths disallows the formation of an integer DD ambiguity by differencing between the two unknown SD ambiguities in Eq. (5b). Therefore, the DD model shown in Eq. (5) becomes Eq. (7).

$$P_{ab}^{RR,ij} = \rho_{ab}^{RR,ij} + I_{ab}^{RR,ij} + T_{ab}^{RR,ij} + \varepsilon_{ab}^{RR,ij}, \tag{7a}$$

$$\lambda^{R,j} \Phi_{ab}^{R,j} - \lambda^{R,i} \Phi_{ab}^{R,i} = \rho_{ab}^{RR,ij} + \lambda^{R,j} N_{ab}^{R,j} - \lambda^{R,i} N_{ab}^{R,i} - I_{ab}^{RR,ij} + T_{ab}^{RR,ij} + \xi_{ab}^{RR,ij}, \tag{7b}$$

where  $R$  indicates that the SD observations are from GLONASS, while  $RR$  refers to that the DD observations are

from GLONASS. This model is not the only approach to solving a GLONASS baseline (Leick 1998; Wang et al. 2001). For example, the observation model can also be expressed in units of cycles, so that the SD ambiguity parameters can be directly combined. In that case, the receiver clock parameters cannot be canceled out, and they must be calculated. However, these various models are similar and can be easily transformed between each other. Moreover, they have been found to exhibit similar performances (Li and Wang 2011; Al-Shaery et al. 2012). Therefore, in this study, we only use the model shown in Eq. (7).

The SD ambiguities  $N_{ab}^{R,i}$  and  $N_{ab}^{R,j}$  in Eq. (7b) are unknown, and the number of those SD ambiguities is larger than the number of the carrier phase DD observations by one. Thus, the NEQ derived from Eq. (7) is rank deficient. However, the pseudorange observations can be used to calculate the initial values of SD ambiguities, eliminating the rank deficiency problem. From the SD models described in Eq. (2b), the SD ambiguity  $N_{ab}^{R,i}$  can be calculated as follows:

$$N_{ab}^{R,i} = -\frac{1}{\lambda^{R,i}} P_{ab}^{R,i} + \Phi_{ab}^{R,i} + \frac{1}{\lambda^{R,i}} (\bar{d}_{ab}^R - \bar{\mu}_{ab}^R + 2I_{ab}^{R,i}). \tag{8}$$

The error in Eq. (8) is as follows:

$$\delta N_{ab}^{R,i} = \frac{1}{\lambda^{R,i}} (\bar{d}_{ab}^R - \bar{\mu}_{ab}^R + 2I_{ab}^{R,i} - \varepsilon_{ab}^{R,i} + \xi_{ab}^{R,i}). \tag{9}$$

In Eq. (9), in addition to the hardware delays ( $\bar{d}_{ab}^R - \bar{\mu}_{ab}^R$ ), the ionospheric delay term  $2I_{ab}^{R,i}$  and the pseudorange observation noise  $\varepsilon_{ab}^{R,i}$  are the main contributors to the ambiguity estimation error  $\delta N_{ab}^{R,i}$ . The  $2I_{ab}^{R,i}$  term can be corrected based on multi-frequency observations, or can be neglected in the case of short baselines. The remaining pseudorange observation noise term  $\varepsilon_{ab}^{R,i}$  depends on the satellite system and the quality of the receivers.

After the SD ambiguities  $N_{ab}^{R,i}$  and  $N_{ab}^{R,j}$  and the corresponding VC matrix (cycles) in the DD model of Eq. (7b) are solved, their DD ambiguities  $N_{ab}^{RR,ij}$  and corresponding VC matrix can be calculated. The wavelength corresponding to the DD ambiguity  $N_{ab}^{RR,ij}$  is neither  $\lambda^{R,i}$  nor  $\lambda^{R,j}$ , but a wavelength between  $\lambda^{R,i}$  and  $\lambda^{R,j}$ . Moreover, the calculated  $N_{ab}^{RR,ij}$  value is affected by the error terms in Eq. (9). This can be clarified by writing the terms  $(\lambda^{R,j} N_{ab}^{R,j} - \lambda^{R,i} N_{ab}^{R,i})$  in Eq. (7b) as  $(\lambda^{R,j} N_{ab}^{RR,ij} - (\lambda^{R,i} - \lambda^{R,j}) N_{ab}^{R,i})$ .

The term  $(\bar{d}_{ab}^R - \bar{\mu}_{ab}^R)$ , the difference between the between-receiver SD hardware delays for pseudorange and carrier phase observations of a channel, in Eq. (9) is involved in GLONASS data processing if the pseudorange observations are used to determine initial values for SD ambiguities or to calculate the receiver clock errors. Thus, the between-

receiver IFB should be corrected if these terms are nonzero. However, the  $(\bar{d}_{ab}^R - \bar{\mu}_{ab}^R)$  term in Eq. (8) is usually unknown and not considered in analyses. By ignoring  $(\bar{d}_{ab}^R - \bar{\mu}_{ab}^R)$ , ISDDAs can be resolved in GLONASS FDMA data processing (Kozlov and Tkachenko 1998; Tian et al. 2015; Banville 2016). Thus, it is reasonable to consider the value of  $(\bar{d}_{ab}^R - \bar{\mu}_{ab}^R)$  to be negligible in Eq. (9), and thus  $\bar{d}_{ab}^R \approx \bar{\mu}_{ab}^R$ .

### 2.2 Inter-system DD model for narrowly spaced frequencies

In this section, we present the inter-system DD model used for observations from different satellite systems with narrowly spaced frequencies. In this case, the SD hardware delays do not cancel each other in the DD model. The inter-system DD model has the form of Eq. (5), with  $s1$  and  $s2$  representing different systems.

As in GLONASS data processing, the resultant normal equation is rank deficient because the number of SD ambiguity parameters in Eq. (7) is one larger than the rank of the DD equations. Hence, the initial SD ambiguity values are necessary to solve the equations. In addition, the initial SD ambiguity value of  $s1$  can be calculated from pseudorange observations based on the SD model (2) and can be expressed as follows:

$$N_{ab}^{s1,i} = -\frac{1}{\lambda^{s1,i}} P_{ab}^{s1,i} + \Phi_{ab}^{s1,i} + \frac{1}{\lambda^{s1,i}} (\bar{d}_{ab}^{s1} - \bar{\mu}_{ab}^{s1} + 2I_{ab}^{s1,i}). \tag{10}$$

Considering the unknown values of  $\bar{d}_{ab}^{s1}$ ,  $\bar{\mu}_{ab}^{s1}$ , and  $I_{ab}^{s1,i}$ , the error of  $N_{ab}^{s1,i}$  in (10) is denoted as  $\delta N_{ab}^{s1,i}$ :

$$\delta N_{ab}^{s1,i} = \frac{1}{\lambda^{s1,i}} (\bar{d}_{ab}^{s1} - \bar{\mu}_{ab}^{s1} + 2I_{ab}^{s1,i} - \varepsilon_{ab}^{s1,i} + \xi_{ab}^{s1,i}). \tag{11}$$

Equations (10) and (11) are generic and are equivalent to Eq. (8) and (9) for GLONASS data processing. In GLONASS FDMA data processing, the SD ambiguities  $N_{ab}^{s1,i}$  and  $N_{ab}^{s2,j}$  in Eq. (5b) are determined and then differenced to produce the DD ambiguity  $N_{ab}^{s1s2,ij}$ . The errors in the initial values of the SD ambiguities  $N_{ab}^{s1,i}$  and  $N_{ab}^{s2,j}$  as presented in Eq. (11) will produce errors in the DD ambiguity  $N_{ab}^{s1s2,ij}$ , because of the wavelength difference. The maximum wavelength difference among the GLONASS L1 frequencies is 0.85 mm. When the GPS L1 and GLONASS L1 signals are integrated, the maximum wavelength difference  $(\lambda^{G,j} - \lambda^{R,i})$  between the two signals is 3.55 mm, 4.18 times larger than that for the GLONASS system alone. This implies that when the GPS L1 and GLONASS L1 signals are integrated, the error in the initial SD ambiguities  $N_{ab}^{R,i}$  and  $N_{ab}^{G,j}$  is also 4.18 times greater than that for the GLONASS L1 data alone. Therefore,

its effect on the determination of the DD ambiguity  $N_{ab}^{RG,ij}$  is also much greater in the GPS L1 and GLONASS L1 integration case. The effect will be detailed further in Sects. 3.2 and 3.3.

If the hardware delay terms  $\bar{d}_{ab}^{s1s2}$  and  $\bar{\mu}_{ab}^{s1s2}$  in Eq. (5) are known, the same processing procedure as that for GLONASS single-system FDMA data can be used to estimate the SD ambiguities in Eq. (5), and thus the DD ambiguities can be calculated. The  $(\bar{d}_{ab}^{s1} - \bar{\mu}_{ab}^{s1})$  term in Eq. (11) is equivalent to  $(\bar{d}_{ab}^R - \bar{\mu}_{ab}^R)$  in GLONASS FDMA data processing. GNSS CDMA signals may be regarded as special cases of GLONASS FDMA signals. Therefore, the  $(\bar{d}_{ab}^{s1} - \bar{\mu}_{ab}^{s1})$  term is approximately negligible in Eq. (10) and (11), and thus  $\bar{d}_{ab}^{s1} \approx \bar{\mu}_{ab}^{s1}$  and  $\bar{d}_{ab}^{s2} \approx \bar{\mu}_{ab}^{s2}$ .

### 2.3 Inter-system bias (ISB)

The between-receiver hardware delays in the DD models result in ISB. Therefore, we used ISB, denoted as  $\bar{d}_{ab}^{s1s2}$  and  $\bar{\mu}_{ab}^{s1s2}$ , to characterize the errors resulting from differences between systems. The ISB  $\bar{d}_{ab}^{s1s2}$  for pseudorange observations can usually be calculated using single point positioning (SPP). The value of  $\bar{\mu}_{ab}^{s1s2}$ , for carrier phase observations, can be numerically decomposed into two parts:

$$\bar{\mu}_{ab}^{s1s2} = \tilde{\mu}_{ab}^{s1s2} + \bar{\lambda} N_{\tilde{\mu}_{ab}^{s1s2}}, \tag{12}$$

where  $\tilde{\mu}_{ab}^{s1s2}$  is the fractional part of the ISB (F-ISB) and is shorter than one wavelength of the signal,  $\bar{\lambda}$  is the wavelength corresponding to the IIDDAs, and  $N_{\tilde{\mu}_{ab}^{s1s2}}$  is an integer.

When GNSS observations of the same frequency are integrated, the integer part of the ISB does not affect ambiguity resolution because the integer  $N_{\tilde{\mu}_{ab}^{s1s2}}$  in Eq. (12) combines with the integer DD ambiguity; therefore, the sum is also an integer. The F-ISB disrupts integer ambiguity resolution when it combines with the DD ambiguity. Therefore, the F-ISB needs to be either removed or estimated.

When GNSS observations of different frequencies are integrated, the integer part of the ISB cannot be neglected. The wavelength corresponding to the DD ambiguity  $N_{ab}^{s1s2,ij}$  determined from the SD ambiguities in Eq. (5b) is not a fixed value, but a value variable between  $\lambda^{s1,i}$  and  $\lambda^{s2,j}$ . The wavelength  $\bar{\lambda}$  in Eq. (12) can change within a single observation period, such as the results presented at the end of Sect. 3.2, because the number of observed satellite varies. Thus, the F-ISB  $\tilde{\mu}_{ab}^{s1s2}$  in Eq. (12) is also variable. However, we expect  $\tilde{\mu}_{ab}^{s1s2}$  to be stable; therefore, its estimated value can be applied to correct observations of multiple observation sessions. Fortunately, the magnitude of the wavelength variation is between  $\lambda^{s1,i}$  and  $\lambda^{s2,j}$ ; thus, this variation is small in our experiments because the frequencies are nar-

rowly spaced. If the integer  $N_{\tilde{\mu}_{ab}^{s1s2}}$  in Eq. (12) is also a small value, the  $\tilde{\mu}_{ab}^{s1s2}$  term will be stable, at least in short term.

Although it is difficult to determine  $N_{\tilde{\mu}_{ab}^{s1s2}}$  in Eq. (12) directly, the value of  $\tilde{\mu}_{ab}^{s1s2}$  is approximately equal to the pseudorange hardware delay  $\bar{d}_{ab}^{s1s2}$  (see Sect. 2.2), and  $\bar{d}_{ab}^{s2,j} \approx \tilde{\mu}_{ab}^{s2,j}$ . Therefore  $\tilde{\mu}_{ab}^{s1s2}$  can be expressed as follows:

$$\tilde{\mu}_{ab}^{s1s2} = \hat{d}_{ab}^{s1s2} + \delta\tilde{\mu}_{ab}^{s1s2}, \tag{13}$$

where  $\hat{d}_{ab}^{s1s2}$  is the pseudorange ISB, determined from pseudorange observations, which can be regarded as an approximation of the carrier phase ISB.  $\delta\tilde{\mu}_{ab}^{s1s2}$  is the difference between the true values of  $\tilde{\mu}_{ab}^{s1s2}$  and  $\hat{d}_{ab}^{s1s2}$ . The term  $\delta\tilde{\mu}_{ab}^{s1s2}$  is unknown, but it will not be large because  $\bar{d}_{ab}^{s1s2,j} \approx \tilde{\mu}_{ab}^{s1s2,j}$ .  $\delta\tilde{\mu}_{ab}^{s1s2}$  can be separated into an integer part and a fractional part. Therefore, the phase ISB can be written as follows:

$$\tilde{\mu}_{ab}^{s1s2} = \hat{d}_{ab}^{s1s2} + \delta\tilde{\mu}_{ab}^{s1s2} + \bar{\lambda}N_{\delta\tilde{\mu}_{ab}^{s1s2}}, \tag{14}$$

where  $\delta\tilde{\mu}_{ab}^{s1s2}$  is a fractional part that is smaller than one wavelength.  $N_{\delta\tilde{\mu}_{ab}^{s1s2}}$  is the integer part, which is neglected.  $\bar{\lambda}$  is the wavelength corresponding to the DD ambiguity  $N_{\tilde{\mu}_{ab}^{s1s2,ij}}$  and has a value between  $\lambda^{s1,i}$  and  $\lambda^{s2,j}$  (Eq. (5b)). The fractional part  $\delta\tilde{\mu}_{ab}^{s1s2}$  is the only value that needs to be accurately estimated and is denoted as F-ISB in the following sections.

### 2.4 Estimation of F-ISB

The F-ISB defined in Sect. 2.3 can be estimated using the particle filter approach proposed by Tian et al. (2016). The particle filter method is based on a Bayesian filter implemented using the Monte Carlo method, which approximates the variables via a simulation with weighted samples. The particle filter-based F-ISB estimation approach is closely related to RATIO value proposed by (Euler and Schaffrin 1991). The RATIO value is calculated by

$$\text{RATIO} = \frac{q(\check{\mathbf{b}}')}{q(\check{\mathbf{b}})} = \frac{\|\hat{\mathbf{b}} - \check{\mathbf{b}}'\|^2 \mathbf{Q}_{\hat{\mathbf{b}}\hat{\mathbf{b}}}}{\|\hat{\mathbf{b}} - \check{\mathbf{b}}\|^2 \mathbf{Q}_{\hat{\mathbf{b}}\hat{\mathbf{b}}}},$$

where  $\hat{\mathbf{b}}$  is the estimated float DD ambiguity vector,  $\check{\mathbf{b}}$  is the primary candidate of the DD integer ambiguity vector,  $\check{\mathbf{b}}'$  is the secondary candidate of the DD integer ambiguity vector, and  $\mathbf{Q}_{\hat{\mathbf{b}}\hat{\mathbf{b}}}$  is the VC matrix of  $\hat{\mathbf{b}}$ .

The particle filter-based F-ISB estimation approach can be summarized as follows. Firstly, the initial range  $[-0.1, 0.1]$  is randomly sampled. The generated samples are used as F-ISB values which substitute  $\delta\tilde{\mu}_{ab}^{s1s2}$  in Eq. (14) stepwise to generate  $\tilde{\mu}_{ab}^{s1s2}$  samples. Secondly,  $\tilde{\mu}_{ab}^{s1s2}$  samples are substituted into Eq. (5b) or its normal equation. The LAMBDA

method is then used to derive the corresponding RATIO values. Thirdly, the weights of the  $\delta\tilde{\mu}_{ab}^{s1s2}$  samples are updated with the normalized RATIO value. Finally, the resampling and prediction steps are conducted, and the cluster analysis method is used to find a solution to the half-cycle problem (Tian et al. 2016). If the filtering converges, the F-ISB  $\delta\tilde{\mu}_{ab}^{s1s2}$  is considered to be accurately estimated and can then be used to calculate the ISB  $\tilde{\mu}_{ab}^{s1s2}$  in Eq. (14). If the observations are contaminated by errors such as the multipath effects and remaining atmospheric delays, the ambiguity fixing will fail even if the ISB is accurately known. In this case, the RATIO distribution cannot show the ISB's information clearly and the filtering may not converge.

## 3 Investigating the relationship between RATIO and ISB

In short baseline data processing, DD models can cancel many types of errors, which leaves the unknown between-receiver ISB and the DD ambiguities for analysis. If the ISB can be sufficiently approximated, the remaining DD ambiguities will be integers, and a large RATIO value can be obtained in the ambiguity fixing. Thus, analyzing the relationship between RATIO and ISB may provide information regarding the remaining ISB or F-ISB in the observation equations.

In this section, the data used in our experiments are first introduced. Then, our investigations into the RATIO distribution with different F-ISB values, and the corresponding ambiguity fixing solutions, are described.

### 3.1 Data description

This section describes the GNSS data (GPS and GLONASS observations) used in this study. These data were obtained from two IGS stations (KOSG and KOS1, located in the Netherlands), separated by about 814 meters. KOSG is equipped with a Leica GRX1200 GG PRO receiver and an AOAD/M\_B antenna. KOS1 is equipped with a Septentrio PolaRx4 receiver and a Leica AR25.R3 antenna. The data were collected on day of year (DOY) 048 of 2014 with a sampling interval of 30 s.

The pseudorange IFB is corrected using the lookup table method described in Sect. 2.1.2. The baseline solutions obtained from pseudorange observations with and without GLONASS IFB corrections are shown in Fig. 1. The assumption that the sum of the SD pseudorange IFBs is zero does not affect the GLONASS solutions, because the DD model rather than the SD model was used for the baseline solutions. In the inter-system DD models, the bias resulting from the zero-sum assumption is combined with the pseudorange

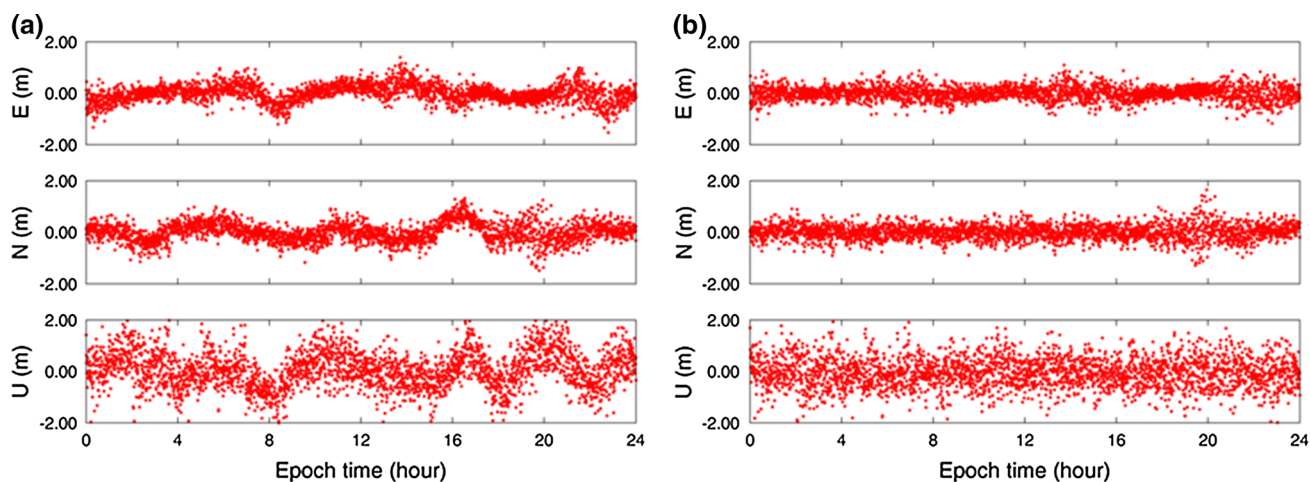


**Fig. 1** Positioning errors in the three components of baseline KOSG–KOS1 determined from GLONASS L1 code pseudorange observations **a** without and **b** with pseudorange IFB correction by pseudorange SD

ISB. This bias can be ignored, because the pseudorange ISB approximates the phase ISB only.

### 3.2 Relationship between RATIO and F-ISB

The investigation of the RATIO distribution with different carrier phase F-ISB values in GPS L1 and GLONASS L1 integration is detailed in this section. First, a range of minimum and maximum carrier phase F-ISB values was defined, from which samples were taken and they were regarded as the actual values of carrier phase F-ISBs. The intra- and inter-system models were used to estimate float ambiguity solutions corresponding to each sample of carrier phase F-ISB. By introducing the initial SD ambiguity values, float DD ambiguities were derived. The RATIO values were then calculated during the ambiguity resolution. The data were processed epoch by epoch, and the satellite (GPS or GLONASS) with the highest elevation was selected as the reference satellite.

Although the carrier phase F-ISB is smaller than the signal wavelength, in the simulation analyses we used a very large F-ISB sampling range of  $[-20, 20]$  m, about 200 times greater than the GPS L1 wavelength (0.19 m). Using a sampling interval of 2 cm, 2000 F-ISB values can be sampled. This enabled an investigation of the influence of F-ISB on RATIO distribution, and the characterization of the periodic characteristics of RATIO distribution. We assumed that the pseudorange and carrier phase ISBs had similar values. The approximate carrier phase ISB was estimated as  $-16.2764$  m, by the SPP method using pseudorange observations. This value was added to the sampled F-ISB values, to reduce the effect of ISB on float DD ambiguity estimation. The corresponding RATIO value was calculated corresponding to each carrier phase ISB value (Fig. 2).

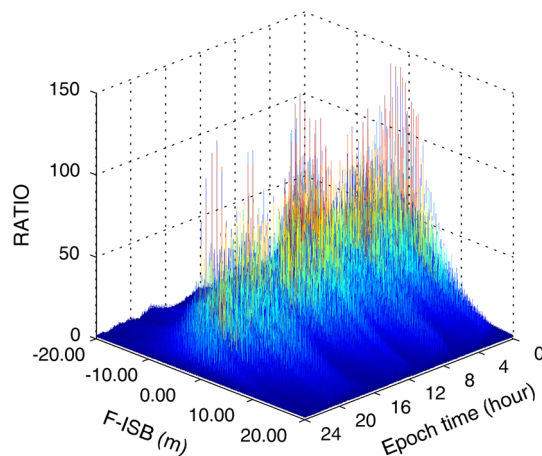


**Fig. 2** Three-dimensional plot of RATIO distribution based on GPS L1 and GLONASS L1 integration and inter-system models for the KOSG–KOS1 baseline

#### 3.2.1 Approximate ISB and F-ISB affect the magnitude of RATIO

Figure 2 shows a ridge composed of local maximum RATIO values in the 3-D RATIO distribution. Local maxima of temporally averaged RATIO values corresponding to each carrier phase F-ISB are evident in Fig. 3a. The local maxima are particularly large when the F-ISB values are small. To better observe the details in Fig. 3a, a smaller sampling range of  $[-1, 1]$  m, and a smaller sampling interval of 1 mm, was defined. In the resulting graph (Fig. 3b), the periodic characteristics of some local maxima can be clearly identified. Because the carrier phase F-ISB was sampled over a large range ( $[-20, 20]$  m), many samples contained an integer multiple of the GNSS signal wavelength. These integer multiples were incorporated into integer ambiguities. When



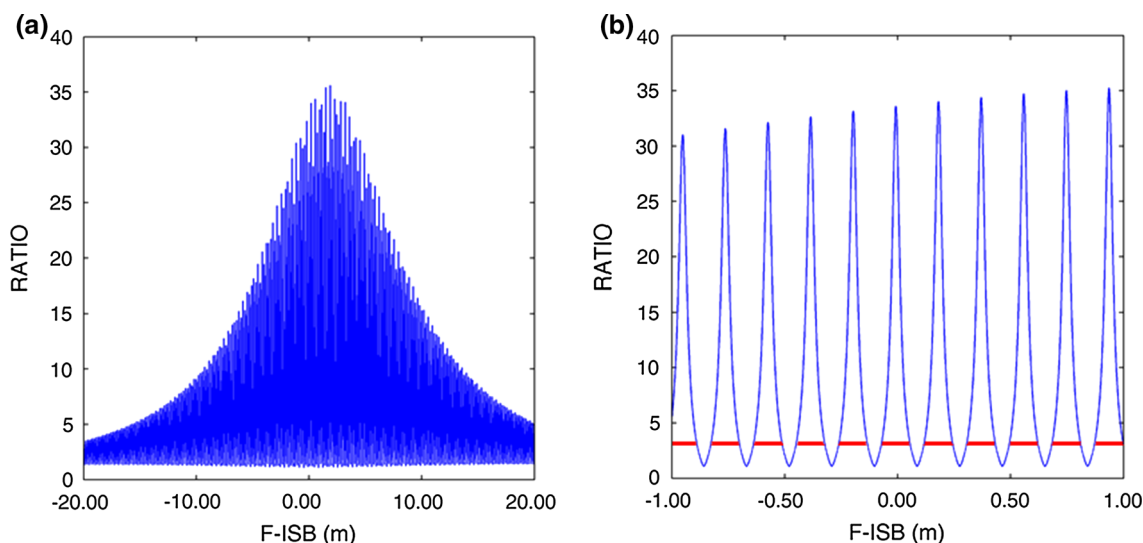


**Fig. 3** **a** RATIO results temporally averaged over 24 hours, corresponding to each carrier phase F-ISB value tested. **b** Magnified region of **a** corresponding to F-ISB vales of  $-1$  to  $1$ . The red line indicates a RATIO value of  $3$

the F-ISB samples had values equal to an exact integer multiple of the wavelength, the estimated DD ambiguities had values close to integers, and the corresponding RATIO values reach local maxima.

The F-ISB samples near the endpoints of the sampling range were affected by larger errors than the samples taken from near the center of the sampling range. These errors affected the estimated SD ambiguities, the IIDDAs, and the GLONASS FDMA ISDDAs. Because the wavelengths of these DD ambiguities differ, the F-ISB sample value cannot be a multiple of all of the different wavelengths simultaneously. Thus, the performance of the ambiguity resolution degraded at these extremely large F-ISB values. In contrast, a ridge of larger RATIO values occurs when F-ISB values are sampled near the central sampling range (Figs. 2 and 3a). Considering that the approximate ISB has been added to the F-ISB samples in the experiments, it is clear that the approximate ISB also affects the magnitude of the RATIO. The true ISB value can maximize the RATIO value. However, only the approximate ISB is known and employed. This can probably explain the ridge’s shift from F-ISB’s zero value in Fig. 3a.

### 3.2.2 Approximate ISB affects the stability of the local maximum RATIO’s location

The wavelength  $\bar{\lambda}$  corresponding to the DD ambiguity is not a fixed value. For example, the distance between two neighboring peaks in Fig. 3b is  $18.87$  cm, which is approximately equal to the average value of the GPS L1 and GLONASS L1 wavelengths. This is because in the GNSS baseline resolution, the contribution of each GNSS system is similar. For instance, both systems have a similar number of observed satellites

and observation weights. If one of the systems is dominant, the distance between two neighboring peaks will change. For example, if there is a full constellation of GPS satellites, but only a single GLONASS satellite, the float SD ambiguity solution will have a small effect on the GPS data, but a significant effect on the GLONASS data, and the distance between two neighboring peaks will approach to the GLONASS L1 wavelength. However, if neither system is dominant, the ISB biases in the inter-system model will affect the SD ambiguity solutions more evenly, and the distance between two neighboring peaks tends toward a value in the middle of the GPS L1 and GLONASS L1 wavelengths.

Experiments with a dominant constellation were implemented using the first hour data collected at KOSG and KOS1 on DOY 048 of 2014 to prove the above description. First, the full GPS constellation and a single GLONASS satellite were selected to estimate the solution. The corresponding RATIO values for each single-epoch solution are shown in the top panel of Fig. 4. RATIO values obtained using data from a single GPS satellite and the full GLONASS constellation are shown in the bottom panel of Fig. 4. For comparison purpose, the RATIO values obtained using full GPS and GLONASS constellations are also shown in both panels. The wavelength of the GLONASS L1 frequency at channel zero is  $18.71$  cm, and the GPS L1 frequency is  $19.03$  cm. Thus, the peaks of the two plots have different F-ISB values on the abscissa axis.

Because, in our analytical method, the approximate ISB  $\hat{a}_{ab}^{s_1s_2}$  is subtracted, the neglected integer part  $N_{\delta\bar{\mu}_{ab}^{s_1s_2}}$  in Eq. (14) is small. This integer part corresponds to the F-ISB samples near to the zero value on the right end of the both panels in Fig. 4. Therefore, regardless of whether the observations from a constellation system are dominant, the RATIO values

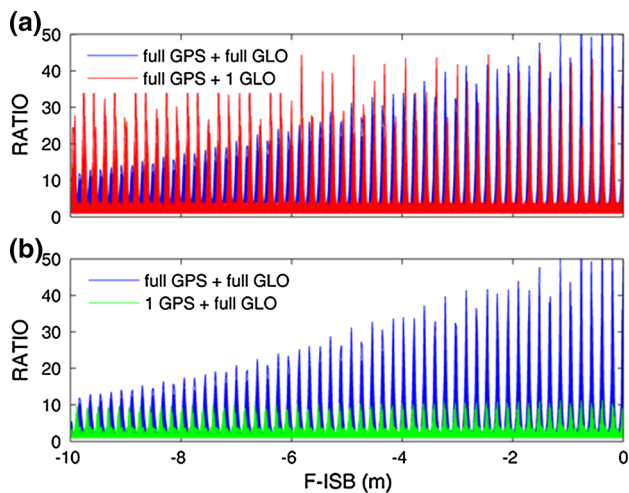


**Fig. 4** Comparisons of RATIO values obtained from integrating full GPS and GLONASS constellations with **a** those obtained from integrating the full GPS constellation and a single GLONASS satellite, and **b** those obtained from integrating a single GPS satellite and the full GLONASS constellation

will exhibit peaks in similar locations to those in Fig. 4. On the right end of the both panels in Fig. 4, the F-ISM is stable and can be estimated from a single scenario and used to correct other scenarios, regardless of the observed constellation. If  $N_{\delta\mu_{ab}^{s1s2}}$  is large, such as in the case where the approximate ISB  $\hat{\mu}_{ab}^{s1s2}$  is not subtracted, the locations of the RATIO peaks on the abscissa axis will vary with different satellite scenarios, as shown on the left end of the both panels in Fig. 4. In this case, the estimated F-ISM value may change with the satellite scenario.

Therefore, both the approximate ISB and F-ISM affect the magnitude and the location of the maximum RATIO. The RATIO value indicates how well the ambiguity's integer nature is recovered. Thus, both the approximate ISB and F-ISM should be considered in the data processing.

### 3.3 Fixed baseline solutions

The ISB remaining in the DD models may result in errors to baseline solutions. Therefore, it is necessary to investigate the variation of baseline solutions with the ISB correction as different values. As in Sect. 3.2, it is necessary to obtain the F-ISM samples and then correct the DD observations using the sampled values plus the approximate ISB. Initially, the F-ISM values are evenly sampled at an interval of 2 cm over a sampling range of  $[-20, 20]$  m. As a typical example, the baseline fixing solutions at the epoch 2871 are presented in Fig. 5.

In Fig. 5, fixed solutions can be obtained with most of the F-ISM samples, except for samples near the endpoints of the range. At the endpoints shown in Fig. 5, the ISB values

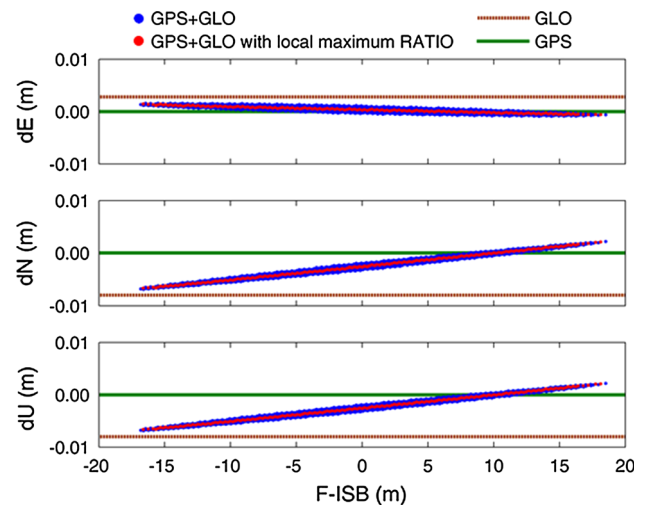


**Fig. 5** Plots showing the influence of the F-ISM value on the baseline fixing solutions of 3-D positioning with respect to a reference 3-D solution. The positioning was conducted at epoch 2871 on DOY 048, 2014, at the KOSG–KOS1 baseline. The reference 3-D positioning solution of this baseline was obtained from a GPS L1 ambiguity-fixed solution. The F-ISM was sampled at an interval of 2 cm in a sampling range of  $[-20, 20]$  m

have relatively large errors. This reduces the accuracy of the float solutions of the SD ambiguities and results in relatively small local maximum RATIO values, and larger errors in the residuals after the DD ambiguities are fixed as integers. Furthermore, the large residual errors significantly affect the fixed baseline solutions, which are estimated with known integer ambiguities. Therefore, the plots in Fig. 5 are not parallel to the abscissa axis. However, the maximum bias in the fixed solutions is only a few millimeters in magnitude, even though the sampled F-ISM value may be as large as 20 m. The plots shown in Fig. 5 indicate that if the F-ISM is smaller than the signal wavelength, which is likely in real-world data, the positioning solutions will have small errors.

To observe the data shown in Fig. 5 in detail, the F-ISM values were resampled over a sampling range of  $[-1, 1]$  m, with a sampling interval of 1 mm. The biases of the ambiguity-fixed solutions for the epoch 2871 with respect to the reference solution are shown in Fig. 6. From these plots, it is evident that ambiguity-fixed solutions can be obtained from most F-ISM values and that the magnitude of the largest bias in these solutions is only a few millimeters.

To preserve the integer nature of DD ambiguities of different GNSS frequencies in the inter-system model, the carrier phase ISB value needs to be known or estimated. The ISB can be regarded as the sum of an approximate ISB and an accurate F-ISM value. The approximate part can be estimated from pseudorange observations alone using the SPP method. The F-ISM, which is shorter than the signal's wavelength, needs to be accurately estimated. The approximate ISB value is

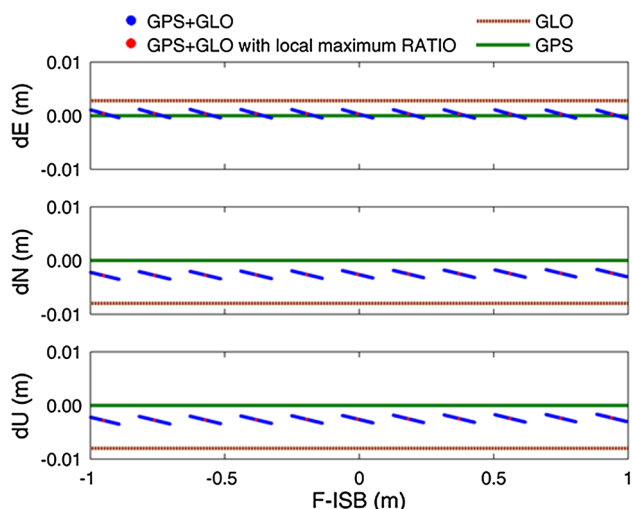


**Fig. 6** Plots of the influence of F-ISB on ambiguity-fixed 3-D positioning solutions with respect to a reference 3-D solution. The positioning was conducted at the epoch 2871 on DOY 048, 2014 at the KOSG–KOS1 baseline. The reference 3-D positioning solution was obtained from a GPS L1 ambiguity-fixed solution. The F-ISB values were sampled from a sampling range of  $[-1, 1]$  m at an interval of 1 mm

important for achieving larger RATIO values (Fig. 3a), and for obtaining more accurate positioning solutions (Fig. 5).

The pseudorange observations were used to calculate the initial SD ambiguity values in the model of Eq. (5b), and thereby eliminate the rank deficiency problem. In the cases of GNSS systems with different frequencies, the errors in the pseudorange observations will be introduced into the initial SD ambiguity values, which will then affect the float DD ambiguities. However, the tolerance of DD ambiguity fixing to the bias in the initial SD ambiguity values is large. As indicated by the red lines in Fig. 3b, the widths of the RATIO peaks at a RATIO value of 3 are 10 ~ 12 cm. This can be regarded as the bias tolerance in the inter-system DD model. Considering the formulation of the model shown in Eq. (10), and that the maximum difference between GPS L1 and GLONASS L1 wavelengths is 3.55 mm, ambiguity-fixed solutions can be obtained if the bias in the initial SD ambiguity value is smaller than 14 m. However, a bias smaller than 14 m does not guarantee the success of ambiguity fixing. Fixed ambiguity solutions also require the use of the intra-system model and adequate observations. Meindl (2011) suggested that the uncertainty of the initial SD ambiguity value should be less than seven cycles (around 1.3 m, in the present study), so that the DD ambiguities can be determined with an error smaller than 0.1 cycles. This condition may be too strict when some intra-system models are included in the estimation. In cases with short baselines and initial SD ambiguity values calculated from pseudorange observations, DD ambiguity fixing can be improved by introducing inter-system DD ambiguity.

## 4 F-ISB estimation and application

This section evaluates the performance of the proposed strategy for fixing both intra- and inter-system DD ambiguities. First, the ISB parameters are estimated where the approximate ISB is calculated from pseudorange observations using the SPP method and is then set as a fixed number. Then, the F-ISB part is derived using the particle filter approach proposed by Tian et al. (2015). At last, the positioning results are analyzed with the calculated F-ISB value, using different elevation masks and constellation geometries.

### 4.1 Estimated F-ISB

As described in Sect. 3, integration of GPS L1 and GLONASS L1 signals using the inter-system models requires knowledge of the ISB value, which can be decomposed into an approximate ISB value plus an accurate F-ISB value. In this experiment, the approximate ISB was estimated as  $-16.2764$  m from pseudorange observations using the SPP method. Then, the F-ISB was estimated using the particle filter method with 24-h data collected at the KOSG–KOS1 baseline on DOY 048 of 2014. The standard deviation of the state noise was set to 1 mm. The estimated F-ISB results are very stable over the 24-h period, as shown in Fig. 7. The insignificant fluctuations were attributed to changes in the observed satellites and atmospheric variations. The average of the estimated F-ISB values was found to be  $-0.0090$  m, and thus the resulting ISB value is  $-16.2854$  m.

An additional experiment was conducted, in which F-ISB values were estimated at the TLSG–TLSE baseline on DOY 001 of 2015, using the inter-system model with GPS L1 and GLONASS L1 integrated observations. The length of baseline TLSG–TLSE is 1266 m. The approximate ISB estimated from pseudorange observations using SPP method is  $-4.9430$  m. The average of the estimated F-ISB values is  $-0.0191$  m, resulting in an ISB value of  $-4.9621$  m.

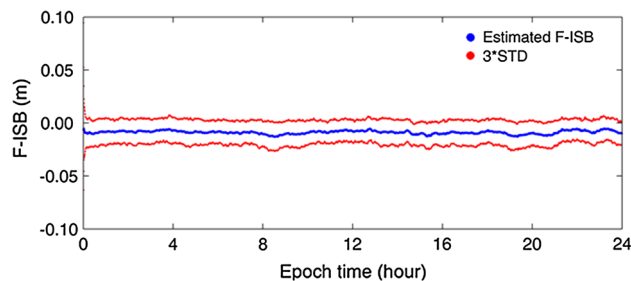


**Fig. 7** Time series of F-ISB values estimated from the integration of GPS L1 and GLONASS L1 data obtained at the KOSG–KOS1 baseline on DOY 048, 2014. The  $3 \times$  standard deviation values of the F-ISB is also shown

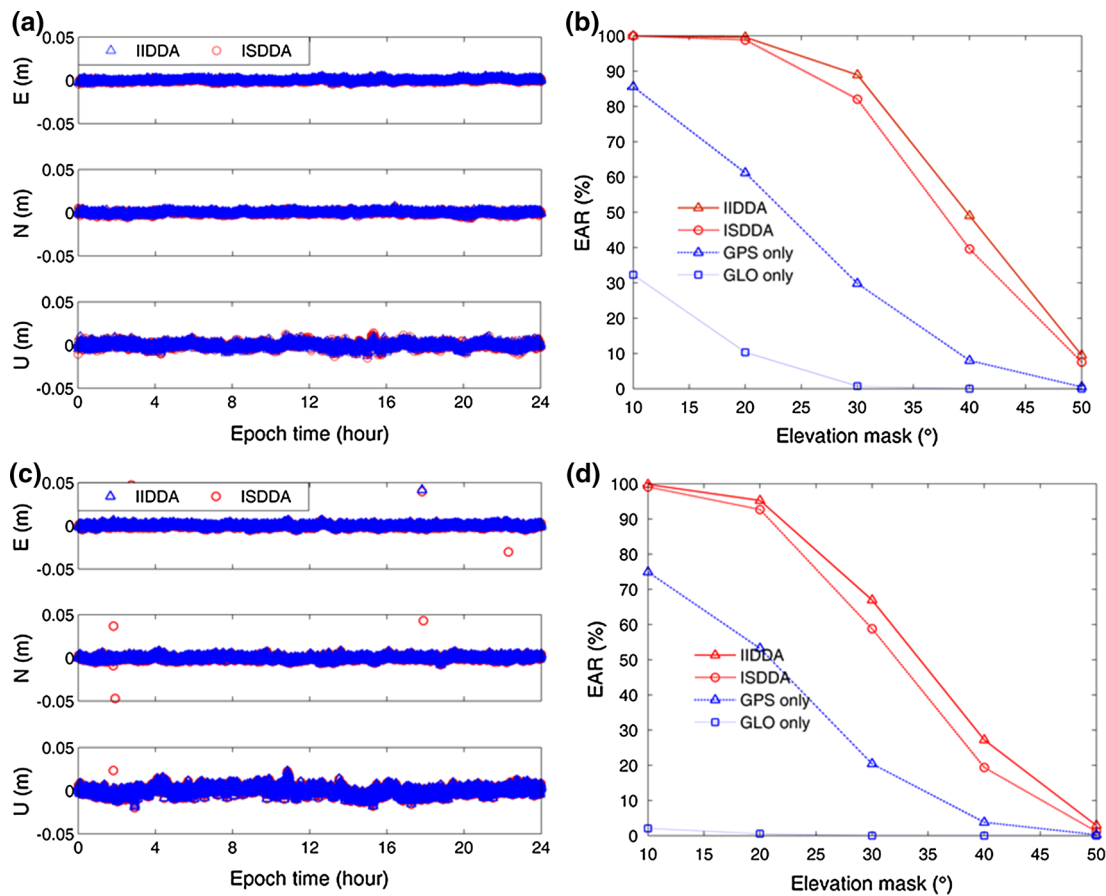


**Fig. 8** 3-D epoch-wise positioning performance using the IISDA and ISDDA fixing strategies in the analyses of GPS L1 and GLONASS L1 data collected on DOY 001, 2015. The GPS-only static solution was used as a reference solution. The results for the KOSG–KOS1 baseline

are shown in **a** and **b**, and the results for the TLSG–TLSE baseline are shown in **c** and **d**. Plots **b** and **d** show the EARs of integer ambiguity fixing at different elevation masks for the two ambiguity fixing strategies and different satellite constellations

## 4.2 Baseline solutions for GPS L1 and GLONASS L1 using inter-system models

This section presents the baseline solutions resolved with known ISB parameters using different ambiguity resolution strategies: fixing IISDA, i.e., GNSS tight integration and fixing only ISDDA, i.e., GNSS loose integration. The baselines were processed using two strategies: (1) using different satellite elevation masks in the data processing and (2) in a challenging observation environment by simulating very severe GNSS satellite signal obstructions. To evaluate the performance of the ambiguity fixing of each testing scenario, we used the empirical availability rate (EAR) used by Li et al. (2015), which is also named success rate such as in Han (1997). EAR is defined as the ratio of the number of epochs with fixed solution to the total number of epochs. Higher EAR values indicate better ambiguity fixing performance.

### 4.2.1 Performance of different ambiguity fixing strategies with different mask angles

Two baselines were solved with both GPS L1 and GLONASS L1 observations by either fixing IISDA or fixing ISDDA. The results for the KOSG–KOS1 and TLSG–TLSE baselines are shown in Fig. 8a and c, respectively. The two sets of results obtained using the two fixing strategies agree well with each other.

Initially, the elevation mask was set to  $10^\circ$ , which enabled 100% of integer ambiguities to be fixed using both strategies. As the elevation mask increases, the number of observed satellites decreases. To investigate how the performance of the strategies varied with different elevation masks, the change in EAR with elevation mask was analyzed (Fig. 8b). The IISDA fixing strategy performed slightly better than the ISDDA fixing strategy. The GPS L1-only baseline solution has a much lower EAR than the GPS L1 and GLONASS L1 integration solution. The GLONASS L1-only baseline solu-

tion is significantly worse than the integrated solution. When the elevation mask was increased significantly, for example, to  $40^\circ$ , the position biases in these solutions are larger than 2 cm horizontally or 3 cm vertically. In this case, the integer ambiguity fixing was considered to be unsuccessful.

The same testing procedure was applied to analyze the TLSG–TLSE baseline with data collected on DOY 001, 2015. With the elevation mask set to  $10^\circ$ , the EAR values obtained from fixing IISDDA and ISDDA were 99.8 and 99.1%, respectively (Fig. 8c). The changes in EAR with different elevation masks for the TLSG–TLSE baseline are shown in Fig. 8d. The EAR obtained from fixing IISDDA was greater than that obtained from fixing ISDDA. The results also show that the GPS and GLONASS integrated solutions are significantly better than GPS-only solutions.

#### 4.2.2 Performance of ambiguity fixing strategies under signal obstruction conditions

To assess the performance of the IISDDA fixing strategy under challenging observation conditions, three analyses were conducted for the KOSG–KOS1 baseline with GPS L1 and GLONASS L1 data collected on DOY 048 of 2014. The obstruction of satellite signals was simulated by disabling the use of some of the satellite data in the GNSS data processing. During data processing, the float SD ambiguities are propagated from one epoch to the next, and DD ambiguity fixing is carried out for each epoch.

In the first simulation, three satellites with elevation angles greater than  $20^\circ$  were selected from each system. The biases of the baseline solutions are shown in Fig. 9. The IISDDA fixing strategy exhibited excellent performance, with an EAR of 93.6%. It is 22.8% higher than the EAR (70.8%) achieved using the ISDDA fixing strategy. The root-mean-square errors (RMSEs) of the positioning results for the two strategies are shown in Table 2. The RMSEs of the results from the IISDDA fixing strategy are significantly smaller than those of the ISDDA strategy results.

Two other obstruction schemes were simulated for the KOSG–KOS1 baseline. First, only data from satellites in the western half of the sky (azimuth  $180^\circ \sim 360^\circ$ ) were used; satellites in the eastern half of the sky (azimuth  $0^\circ \sim 180^\circ$ ) were considered to be obstructed. Conversely, in the second simulation, only data from the satellites with azimuth  $0^\circ \sim 180^\circ$  were used. In both scenarios, the elevation mask was set to  $15^\circ$ , and the results of these two simulations are shown in Fig. 10.

Using the IISDDA fixing strategy, the EAR improved from 85.3 to 90% in the western-sky simulation, and from 81.7 to 93% in the eastern-sky simulation, compared with the results obtained using the ISDDA fixing strategy. The RMSEs of these results are shown in Table 2. Overall, the results of

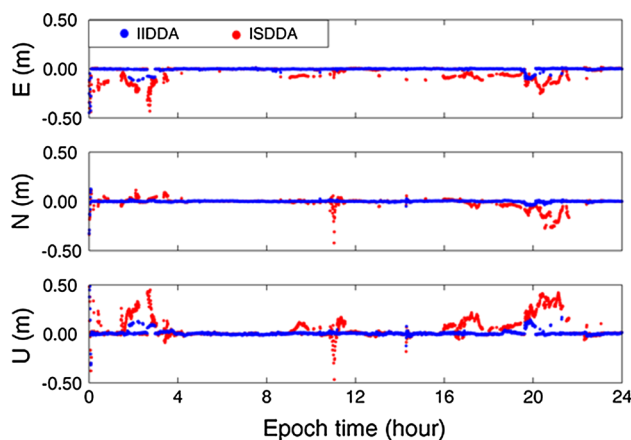


**Fig. 9** 3-D positioning errors of baseline solutions with respect to the GPS-only static reference solution for the KOSG–KOS1 baseline. To simulate challenging observation conditions, data from only three GPS satellites and three GLONASS satellites were used

IISDDA fixing were found to be more accurate and reliable than those of ISDDA fixing.

The IISDDAs of the inter-system model can be fixed as integers in the same way as other multi-GNSS signals of different frequencies are integrated. In the present study, GPS L1 and GLONASS L1 signals were used, with frequency differences of 3–4 mm. The GNSS signal frequencies shown in Table 1 demonstrate that the wavelength differences between different signals may be smaller. The integration of GNSS signals with smaller wavelength differences would improve 3-D GNSS positioning performance.

## 5 Conclusions

In the present study, we developed an approach to estimate the ISB of narrowly spaced frequencies in multi-GNSS signal integration. After the carrier phase ISB is estimated, it can be used as known value in the inter-system model. Thus, the performance of fixing both ISDDA and IISDDA can be improved. The ISB can be decomposed into an approximate ISB, an integer part and an accurate fractional ISB (F-ISB) value. The approximate ISB can be estimated from SPP using pseudorange observations. The integer part combines with the DD ambiguities. The F-ISB can be estimated using the particle filter approach.

Compared to the strategy of fixing ISDDA, where ISB does not exist, the strategy of fixing IISDDA using the estimated ISB in multi-GNSS integration achieves better performance. This approach was tested at the KOSG–KOS1 baseline (length: 814 m) using GPS L1 and GLONASS L1 integration. When three satellites with elevation angles  $> 20^\circ$  are available from each system, the rate of IISDDA fixing is 93.6%, which is 22.8% higher than the rate for ISDDA fixing

**Table 2** RMSEs of 3-D GNSS positioning using ISDDA and IIDDA fixing strategies

	RMSEs of ISDDA fixing (m)				RMSEs of IIDDA fixing (m)			
	E	N	U	3D	E	N	U	3D
3 GPS + 3 GLO	6.4	4.8	10.9	13.5	2.0	0.7	2.4	3.2
GPS + GLO (azimuth $0^\circ - 180^\circ$ )	43.8	8.1	44.9	63.2	1.9	1.7	3.7	4.5
GPS + GLO (azimuth $180^\circ - 360^\circ$ )	5.6	2.8	6.6	9.1	2.3	1.9	2.5	3.9

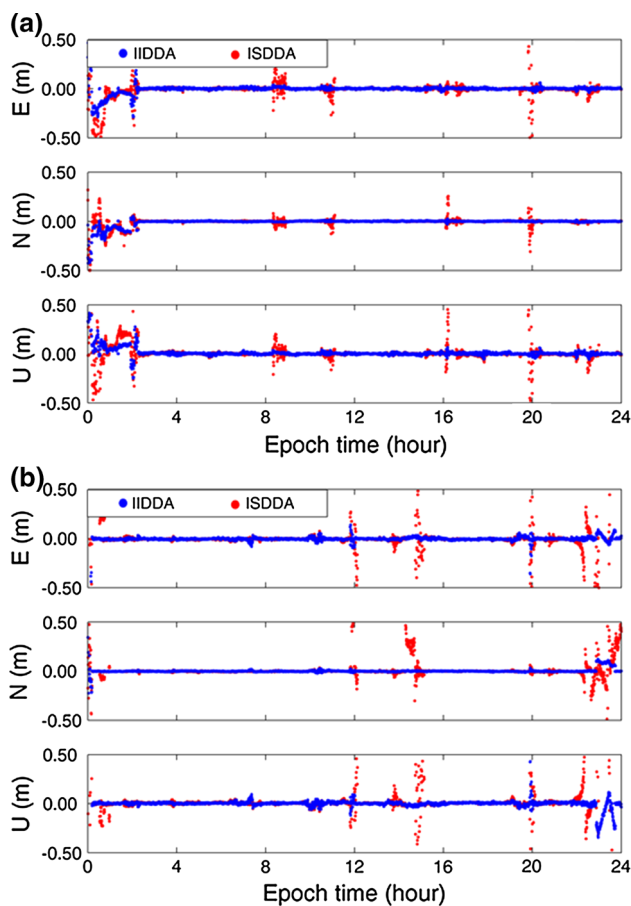


**Fig. 10** Coordinate differences of the KOSG-KOS1 baseline solutions with respect to the GPS-only static reference solution, for satellites observed **a** in the western half of the sky, and **b** in the eastern half of the sky

alone (70.8%). In the GNSS signal obstruction simulations, the empirical success rates of the IIDDA fixing strategy were 4.7 and 11.3% higher than those of ISDDA fixing, when using data from satellites in the eastern and western halves of the sky, respectively. Those improvements may vary for different baselines depending on the multipath effects and baseline lengths.

Besides, the performance of ambiguity fixing (either inter-system ambiguity fixing or intra-, inter-system ambiguity fixing) for narrowly spaced frequencies in multi-GNSS integration can be degraded by errors in the initial SD ambiguity

values. These values are used to remove the rank deficiency problem and are typically estimated by SPP using pseudorange observations. Therefore, minimizing the errors in these initial SD ambiguity values requires further research.

**Acknowledgements** Yumiao Tian was financially supported by the China Scholarship Council (CSC) during his studies at the Technische Universität Berlin, Germany, and the German Research Center of Geosciences (GFZ), Germany. Zhizhao Liu thanks the grant supports from the National Natural Science Foundation of China (Grant NSFC 41274039), the Hong Kong Research Grants Council (RGC) Early Career Scheme (ECS) (Project PolyU 5325/12E (F-PP0F)), and the Hong Kong Polytechnic University (Project 4-BCBT).

## References

- Alber C, Ware R, Rocken C, Braun J (2000) Obtaining single path phase delays from GPS double differences. *Geophys Res Lett* 27(17):2661–2664. <https://doi.org/10.1029/2000GL011525>
- Al-Shaery A, Zhang S, Lim S, Rizos C (2012) A comparative study of mathematical modelling for GPS/GLONASS real-time kinematic (RTK). In: Proceedings of ION GNSS 2012, Nashville, TN, September 2012, pp 2231–2238
- Banville S (2016) GLONASS ionosphere-free ambiguity resolution for precise point positioning. *J Geod* 90(5):487–496. <https://doi.org/10.1007/s00190-016-0888-7>
- Cai C, Gao Y (2013) Modeling and assessment of combined GPS/GLONASS precise point positioning. *GPS Solut* 17(2):223–236. <https://doi.org/10.1007/s10291-012-0273-9>
- Doucet A, Freitas N, Gordon N (2001) Sequential Monte Carlo methods in practice. Springer, New York
- Euler H, Schaffrin B (1991) On a measure of discernibility between different ambiguity solutions in the static-kinematic GPS-mode. In: Proceedings of the international symposium on kinematic systems in geodesy, surveying, and remote sensing. Springer, New York, pp 285–295
- Force D, Miller J (2013) Combined global navigation satellite systems in the space service volume. In: Proceedings of the ION international technical meeting, San Diego, California
- Gordon J, Salmond J, Smith F (1993) Novel approach to nonlinear/non-Gaussian Bayesian state estimation. *IEE Proc F (Radar Signal Process)* 140(2):107–113. <https://doi.org/10.1049/ip-f-2.1993.0015>
- Han S (1997) Quality-control issues relating to instantaneous ambiguity resolution for real-time GPS kinematic positioning. *J Geod* 71(6):351–361. <https://doi.org/10.1007/s001900050103>
- Julien O, Alves P, Cannon E, Zhang W (2003) A tightly coupled GPS/GALILEO combination for improved ambiguity resolution. In: Proceedings of the European Navigation Conference, pp 1–14
- Kozlov D, Tkachenko M (1998) Centimeter-level, real-time kinematic positioning with GPS + GLONASS C/A receivers. *Navigation* 45(2):137–147. <https://doi.org/10.1002/j.2161-4296.1998.tb02378.x>

- Kozlov D, Tkachenko M, Tochilin A (2000) Statistical characterization of hardware biases in GPS + GLONASS receivers. *Proc ION GPS 2000*:817–826
- Leick A (1998) GLONASS satellite surveying. *J Surv Eng-ASCE* 124(2):91–99. [https://doi.org/10.1061/\(ASCE\)0733-9453\(1998\)124:2\(91\)](https://doi.org/10.1061/(ASCE)0733-9453(1998)124:2(91))
- Li T, Wang J (2011) Comparing the mathematical models for GPS and GLONASS integration. In: *Proceedings of international global navigation satellite systems society symposium-IGNSS*, Sydney, Australia
- Li X, Ge M, Dai X, Ren X, Fritsche M, Wickert J, Schuh H (2015) Accuracy and reliability of multi-GNSS real-time precise positioning: GPS, GLONASS, BeiDou, and Galileo. *J Geod* 89(6):607–635. <https://doi.org/10.1007/s00190-015-0802-8>
- Meindl M (2011) Combined analysis of observations from different Global Navigation Satellite Systems. PhD thesis. Astronomisches Institut der Universität Bern, Geodätisch-geophysikalische Arbeiten in der Schweiz
- Melgard T, Tegedor J, Jong K, Lapucha D, Lachapelle G (2013) Interchangeable integration of GPS and Galileo by using a common system clock in PPP. In: *Proceedings of ION GNSS*, Nashville, TN, pp 16–20
- Montenbruck O, Steigenberger P, Khachikyan R, Weber G, Langley R, Mervart L, Hugentobler U (2014) IGS-MGEX: preparing the ground for multi-constellation GNSS science. *Inside GNSS* 9(1):42–29
- Nadarajah N, Khodabandeh A, Teunissen P (2015) Assessing the IRNSS L5-signal in combination with GPS, Galileo, and QZSS L5/E5a-signals for positioning and navigation. *GPS Solut* 20(2):289–297. <https://doi.org/10.1007/s10291-015-0450-8>
- Odiijk D, Teunissen P (2013a) Characterization of between-receiver GPS-Galileo inter-system biases and their effect on mixed ambiguity resolution. *GPS Solut* 17(4):521–53. <https://doi.org/10.1007/s10291-012-0298-0>
- Odiijk D, Teunissen P (2013b) Estimation of differential inter-system biases between the overlapping frequencies of GPS, Galileo, BeiDou and QZSS. In: *Proceedings of the 4th international colloquium scientific and fundamental aspects of the Galileo programme*, Prague, Czech Republic, pp 4–6
- Odiijk D, Teunissen P, Khodabandeh A (2014) Galileo IOV RTK positioning: standalone and combined with GPS. *Surv Rev* 46(337):267–277. <https://doi.org/10.1179/1752270613Y.0000000084>
- Odolinski R, Teunissen P, Odiijk D (2014) Combined BDS, Galileo, QZSS and GPS single-frequency RTK. *GPS Solut* 19(1):151–163. <https://doi.org/10.1007/s10291-014-0376-6>
- Paziewski J, Wielgosz P (2015) Accounting for Galileo-GPS inter-system biases in precise satellite positioning. *J Geod* 89(1):81–93. <https://doi.org/10.1007/s00190-014-0763-3>
- Teunissen PJG, Kleusberg A (1998) GPS observation equations and positioning concepts. In: Teunissen PJG, Kleusberg A (eds) *GPS for geodesy*. Springer, Berlin, Heidelberg, pp 187–229. [https://doi.org/10.1007/978-3-642-72011-6\\_5](https://doi.org/10.1007/978-3-642-72011-6_5)
- Tian Y, Ge M, Neitzel F (2015) Particle filter-based estimation of inter-frequency phase bias for real-time GLONASS integer ambiguity resolution. *J Geod* 89(11):1–14. <https://doi.org/10.1007/s00190-015-0841-1>
- Tian Y, Ge M, Neitzel F, Zhu J (2016) Particle filter-based estimation of inter-system phase bias for real-time integer ambiguity resolution. *GPS Solut*. <https://doi.org/10.1007/s10291-016-0584-3>
- Verhagen S, Teunissen P (2013) The ratio test for future GNSS ambiguity resolution. *GPS Solut* 17(4):535–548. <https://doi.org/10.1007/s10291-012-0299-z>
- Wang J, Rizos C, Stewart M, Leick A (2001) GPS and GLONASS integration: modeling and ambiguity resolution issues. *GPS Solut* 5(1):55–64. <https://doi.org/10.1007/PL00012877>
- Wanninger L (2012) Carrier-phase inter-frequency biases of GLONASS receivers. *J Geod* 86(2):139–148. <https://doi.org/10.1007/s00190-011-0502-y>